Anomalous supercurrent from Majorana states in topological insulator Josephson junctions

Citation: Potter, Andrew C., and Liang Fu. "Anomalous Supercurrent from Majorana States in Topological Insulator Josephson Junctions." Phys. Rev. B 88, no. 12 (September 2013). © 2013 American Physical Society

As Published: http://dx.doi.org/10.1103/PhysRevB.88.121109

Publisher: American Physical Society

Persistent URL: http://hdl.handle.net/1721.1/88776

Version: Final published version: final published article, as it appeared in a journal, conference proceedings, or other formally published context

PHYSICAL REVIEW B **88**, 121109(R) (2013)

Anomalous supercurrent from Majorana states in topological insulator Josephson junctions

Andrew C. Potter[1] and Liang Fu[2]
[1]*Department of Physics, University of California, Berkeley, California 94720, USA*
[2]*Department of Physics, Massachusetts Institute of Technology, Cambridge, Massachusetts 02139, USA*
(Received 9 April 2013; published 30 September 2013)

We propose a Josephson junction setup based on a topological insulator (TI) thin film to detect Majorana states that exploits the unique helical and extended nature of the TI surface state. When the magnetic flux through the junction is close to an integer number of flux quanta, Majorana states, present on both surfaces of the film, give rise to a narrow peak-dip structure in the current-phase relation by hybridizing at the edge of the junction. Remarkably, the maximal Majorana-state contribution to Josephson current takes a (nearly) universal value, approximately equal to the supercurrent capacity of a single quantum channel. These features provide a characteristic signature of Majorana states based entirely on supercurrent.

DOI: 10.1103/PhysRevB.88.121109 PACS number(s): 71.10.Pm, 74.50.+r, 74.90.+n, 73.23.−b

Majorana bound states in superconductors are localized quasiparticles that are equal weight superposition of electron and hole, which have non-Abelian braiding statistics.[1,2] The presence of Majorana bound states can produce unusual transport phenomena such as a 4π-periodic Josephson effect,[3–5] resonant Andreev reflection,[6] and inherently nonlocal transport.[7] Over the last few years, proposals for realizing Majorana states in various superconducting solid-state systems have sparked tremendous interest and intensive activity (see Refs. 8 and 9 and references therein).

Among the proposed material systems for realizing Majorana states, the superconductor (S)-topological insulator (TI) hybrid structure[10] has several distinctive advantages. First, as a parent phase for Majorana states, the S-TI interface is topologically nontrivial even at zero magnetic field. Consequently, the induced superconductivity on the topological surface states of a TI is immune to disorder.[11] This provides a robust route to realizing Majorana states at elevated temperatures.[12] Second, by their topological nature, surface states of a TI extend throughout the entire sample boundary. The extended nature of such states motivates us to propose a setup based on TI thin films for detecting Majorana states. We also note that extended surface states are crucial for realizing Majorana states in TI nanowires.[13,14]

In this paper, we study anomalous Josephson current signatures of Majorana states in a S-TI-S junction under an applied magnetic field, see Fig. 1(a). Importantly, we require that proximity-induced superconductivity exists on both top and bottom surfaces of the TI thin film. This can be achieved when both surfaces are in direct contact with superconductors, or alternatively, when a superconductor is deposited only on one surface, and the superconductivity is transmitted to the other surface either through the bulk states[15] or around the side surfaces (as demonstrated experimentally).[16] Supercurrent through such SC-TI-SC junctions has been recently observed.[17–22]

Our main findings and the basic physics behind them can be stated in simple terms. Applying a magnetic field to the S-TI-S junction induces a one-dimensional array of Josephson vortices (one for each flux quantum piercing the junction). Each vortex traps two localized Majorana states,[10,23] one on each the top and bottom surfaces of the TI. The two are aligned vertically (see Fig. 1). The global phase offset $\theta_{y=0}$ defined at a reference point $y = 0$ is an independent variable, which can be controlled in a SQUID geometry. For a given magnetic field, increasing θ_0 shifts the positions of the vortices and their bound Majorana states along the junction towards one edge of the TI sample. As a Josephson vortex approaches the edge, the wave functions of the Majorana states on the top and bottom surfaces overlap on the *side* surface. The states thereby hybridize, splitting from zero energy and eventually annihilating each other.

This phase dependent splitting gives rise to a supercurrent carried by the Majorana states. When the magnetic flux through the junction is (close to) an integer multiple of flux quanta, the normal contribution to the supercurrent oscillates with position y along the junction and (nearly) cancels, and the supercurrent carried by the Majorana states can dominate. This leads to a narrow peak in Josephson current as a function of phase difference [see Fig. 2(d)].

Model and Majorana bound states. We now derive the Majorana states and the Josephson current-phase relation for a *short* S-TI-S junction, under the condition $W < \xi$, where W is the width of the junction and ξ is the coherence length of topological surface states with proximity-induced superconducting gap. Moreover, we consider the case that the length of the junction, L, is smaller than the Josephson penetration length, so that the self-field from the Josephson current is negligible.[20]

The Hamiltonian for the top surface of the S-TI-S junction is

$$H = \int d^2\mathbf{r}\psi^\dagger(\mathbf{r})\left[v\hat{z}\cdot(\boldsymbol{\pi}\times s) - \mu(\mathbf{r})\right]\psi(\mathbf{r}) + \left[\Delta(\mathbf{r})\psi^\dagger_\uparrow(\mathbf{r})\psi^\dagger_\downarrow(\mathbf{r}) + \text{H.c.}\right]. \quad (1)$$

Here, $\pi_j = -i\partial_j - eA_j(\mathbf{r})$ $(j = x, y)$ and $\psi(\mathbf{r}) = (\psi_\uparrow(\mathbf{r}), \psi_\downarrow(\mathbf{r}))$ describes the TI surface states, which have a Dirac dispersion with Fermi velocity v. Due to doping from the superconductors, the chemical potential in the superconducting region $\mu(\mathbf{r}) = \mu'$ at $|x| > W/2$ is different from the junction area $\mu(\mathbf{r}) = \mu$ at $|x| < W/2$. $A_j(\mathbf{r})$ is the vector potential associated with the magnetic field B. It is convenient to work in the Landau gauge $A_x = 0$. $A_y(\mathbf{r})$ is then given by $A_y(\mathbf{r}) = -Bx$ for $|x| < W/2$, $-BW/2$ for $x > W/2$, and $BW/2$ for $x < -W/2$. In this gauge,

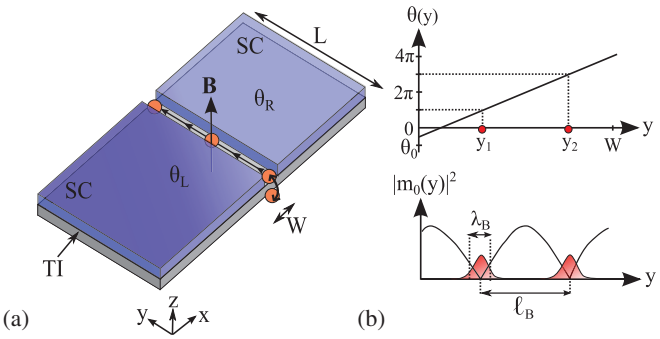

FIG. 1. (Color online) (a) Depiction of the device geometry considered in the text. The top surface of the topological insulator (grey layer labeled TI) is in contact with the superconductors (blue layers), and the superconductivity is transmitted to the bottom surface through the bulk states. As the global-phase offset between the left and right superconductors ($\theta_0 = \theta_R - \theta_L$) is adjusted, Majorana modes (shown as red-circles) bound to Josephson vortices are created at one end of the junction, move along the junction, and fuse on the opposite side of the junction. (b) Local phase difference θ_y for along the junction $3\Phi_0 > \Phi_B > 2\Phi_0$ and fixed θ_0, and the corresponding mass term of Eq. (2). Wherever $\theta_y = \pi \mod 2\pi$, there is a local gap closing that binds a Majorana state.

the superconducting gap is $\Delta(\mathbf{r}) = \Delta e^{i\theta_y/2}$ for $x > W/2$, $\Delta e^{-i\theta_y/2}$ for $x < -W/2$, and 0 for $|x| < W/2$. The phase winding $\theta_y = \pi y/l_B$ ensures zero supercurrent along the y direction in the superconducting region. Here, the magnetic length is defined as $l_B = L\frac{\Phi_0}{\Phi_B}$, where Φ_B is the magnetic flux through the junction.[24]

Since $\Delta(\mathbf{r})$ varies slowly with the position y, we use a semiclassical method to first solve the Hamiltonian without

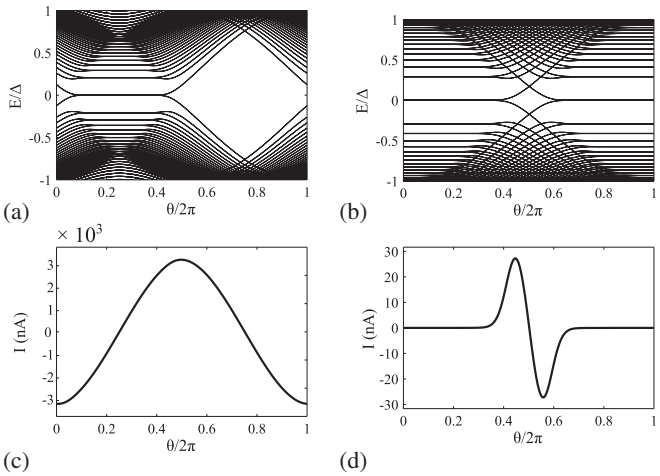

FIG. 2. Numerical computation of the Andreev bound-state spectrum, and Josephson current for Eq. (2) with the parameters $v_F = 4.2 \times 10^5$ m/s, $\mu = 10$ meV, $\Delta = 151$ μeV, and $L = 2$ μm relevant for Al/Bi_2Se_3/Al junctions. (a) and (b) Low-lying Andreev bound-state spectrum as a function of phase difference θ between the superconductors for $\Phi_B = 0.5\Phi_0$ and $\Phi_B = \Phi_0$, respectively. The Josephson current corresponding to (a) and (b) is shown in (c) and (d), respectively. (d) The characteristic sharp peak-dip structure from topological Andreev bound states fusing at the edge of the junction, as discussed in the text.

the kinetic energy term $-iv\partial_y s_x$ at an arbitrary y. This one-dimensional problem was previously solved for TI Josephson junctions[10] and for a related problem in graphene.[25] When the junction length W is shorter than the coherence length $\xi \equiv v/\Delta$, there is a single pair of subgap Andreev bound states at energy $\pm E(y)$, where $E(y) = \Delta\cos(\theta_y/2)$ depends on the local phase difference and oscillates with the position y [see Fig. 1(b)].

Taking the kinetic energy along the y direction into account gives the following effective Hamiltonian for the junction, written in terms of two branches of counterpropagating Majorana fermions $\gamma_{L,R}$,[10]

$$H_{\text{eff}} = iv_M(\gamma_L\partial_y\gamma_L - \gamma_R\partial_y\gamma_R) + iE(y)\gamma_L\gamma_R. \qquad (2)$$

The velocity v_M depends on intrinsic properties of the junction. For a ballistic junction, it was found that $v_M \simeq v(\Delta/\mu)^2$ for $\mu = \mu'$ in Ref. 10 and $v_M \simeq v(\Delta/\mu)\sin(\mu W/v)$ for $\mu \ll \mu'$ in Ref. 25.

To analytically examine the Majorana bound-state structure, it is instructive to consider the region near a level crossing point $y = y_1$, where $E(y) \approx \pi\Delta(y - y_1)/l_B$. The bound-state energy $E(y)$ corresponds to the hybridization between the two Majorana states and vanishes linearly at $y = y_1$. The sign reversal of $E(y)$ as a function of y gives rise to a zero-energy Majorana bound state that is spatially localized in the junction at the position y_0. The corresponding Majorana operator γ_1 is given by

$$\gamma_1 = \int dy \frac{e^{-(y-y_1)^2/2\lambda_B^2}}{\sqrt{2\pi\lambda_B^2}} \frac{1}{\sqrt{2}}[\gamma_L(y) + \gamma_R(y)], \qquad (3)$$

where the decay length in the y direction λ_B is $\lambda_B = \sqrt{v_M l_B/\pi\Delta}$. This Majorana state is confined by the TI band gap in the z direction, the proximity-induced superconducting gap in the x direction, and the magnetic field induced linear potential $E(y)$ in the y direction. The decay length in the z direction is given by the penetration depth of topological surface states into the bulk, which is typically a few nanometers. The decay length in the x direction is given by the coherence length ξ (typically a few hundred nanometers). Since Δ/μ is typically of the order 10^{-3}, the decay length of Majorana states λ_B along the junction is much smaller than their separation, and the overlap of two Majorana states along the junction is negligible, except when a pair of them nears the edge of the TI.

Near each π crossing, the zero-energy Majorana state is accompanied by other nonzero energy Andreev bound states (ABS's). Approximating the mass term by a linear potential, $E(y) = \pi\Delta(y - y_1)/\ell_B$ [valid in the vicinity of $\theta(y) \approx \pi$], these ABS's have energies $\pm E_n$, where $E_n \approx \sqrt{2\pi n v_M\Delta/l_B}$, $n = 1, 2, \ldots, n_{\max}$, and $n_{\max} \approx \ell_B\Delta/v_M$.

We also support this analytical picture by numerically computing the spectrum of Andreev bound states discretizing (2) on a finite lattice of spacing a, with $E(y) \approx \Delta\cos(\frac{\pi y}{\ell_B})$. In this simulations, we used realistic parameters of v_F and Δ for an Al/Bi_2Se_3/Al junction and junction geometry comparable to that in Refs. 20–22. While μ for Bi_2Se_3 is typically ≈0.1 eV, for simplicity, we illustrate the case for smaller $\mu \approx 10$ meV, which can readily be achieved by gating.[17,22] The Andreev bound-state spectra are shown in Fig. 2 for half a magnetic

flux quantum [panel (a)] and a single magnetic flux quantum [panel (b)], and are well described by the simplified analytical picture developed above.

Contrast to conventional junctions. Low-energy Andreev bound states can also occur near the π phase difference in conventional metallic Josephson junctions under ideal conditions. For a transparent superconductor-normal interface, and in the absence of spin-orbit coupling, a conventional 2D metallic junction can be thought of as two separate copies of Eq. (2), one for right-moving spin-up electrons and left-moving spin-down holes, and another for the corresponding time-reversed partners. This would lead to low-energy ABS's bound to Josephson vortices similar to those described above, except doubly degenerate.

However, in practice, normal scattering at the S-N interface (for example, due to the chemical potential mismatch in S and N regions) and spin-orbit coupling will push ABS up in energy towards the bulk gap Δ, and even completely remove them in a short Josephson junction. In contrast, the helical nature of the TI surface state gives rise to topologically protected ABS's. Therefore, in the short-junction limit, the Josephson signatures described below are particular to the special properties of the S-TI-S junction.

Josephson current. Having discussed the structure of low-energy Andreev bound states in the junction, we now analyze their effect on Josephson current. When the number of magnetic flux quanta, Φ_B/Φ_0, is not close to a nonzero integer then the Josephson current is carried predominately by conventional Andreev bound states (at nonzero energy) and shows a close-to-sinusoidal current-phase dependence [see Fig. 2(a)]. Near integer values of flux quanta, $\Phi_B/\Phi_0 = \pm 1, \pm 2, \ldots$, however, the conventional contribution becomes vanishingly small. (It is noted that away from an integer number of flux quanta, the Majorana states still contribute to the Josephson current near $\theta = \pi$, however, this contribution is covered by a large background from normal ABS's. It would be interesting to think alternative setups to subtract this background.)

In this regime, the Majorana bound-state contribution to Josephson current dominates. For simplicity, we will first describe the situation for $\Phi_B = \Phi_0$ [see Fig. 2(b)]. The case of $\Phi_B = N\Phi_0$ is similar. When $\Phi_B = \Phi_0$, and $\theta_0 \neq \pi$, there is exactly one Josephson vortex piercing the junction, which binds Majorana modes at $y_0 = \frac{L}{2}(1 - \frac{\theta_0}{\pi})$ on both the top and bottom surfaces of the TI. These Majorana modes hybridize by tunneling into each other around the perimeter of the junction. The resulting energy splitting is exponentially suppressed as $e^{-2\min[y_0,(L-y_0)]/\lambda_B}$ and is negligibly small when the position of Majorana modes y_0 is more than a few λ_B away from the edges of the junction. In this regime, the splitting is insensitive to y_0 and θ_0, and the Majorana modes do not contribute to the Josephson current.

In contrast, when $\theta_0 \approx \pi$, $y_0 \approx 0$ and the Majorana states are strongly coupled near the edge and split away from zero-energy. If the junction height $h \lesssim \lambda_B$, then we may ignore then finite thickness of the TI film, and the Majorana states are split by energy $\delta E_M \approx \sqrt{\frac{v_M \Delta}{\ell_B}}$. As θ_0 approaches π from below, the Majorana states move towards the junction edge at $y = 0$ and begin to fuse and split when $\theta_0 \approx \pi(1 - \frac{\lambda_B}{L})$. Increasing θ_0 beyond π causes a different set of Majorana states to emerge from near $y = L$, and move to decreasing y, reversing the process that occurred near $y = 0$ for $\theta_0 > \pi$. The hybridization of Majorana states at the two edges gives rise to local supercurrents in *opposite* directions. At $\theta_0 = \pi$, the splitting of Majorana states is large, but supercurrents from two edges cancel. Slight deviation from $\theta_0 = \pi$ tips the balance by increasing the magnitude of supercurrent at one edge and suppressing the other, thereby generating a nonzero total supercurrent. The sensitivity of the Majorana splitting energy to the phase difference implies that the Majorana states contribute a peak in the Josephson current near $\phi_0 \approx \pi(1 - \frac{\lambda_B}{L})$ followed by a dip in the Josephson current near $\phi_0 \approx \pi(1 + \frac{\lambda_B}{L})$ [see Fig. 2(d)].

By these considerations, we find that the maximal supercurrent from the fusion of Majorana states is $I_M = \max[\frac{2\pi}{\Phi_0}\frac{\partial E}{\partial \theta_0}] \approx \Delta/\Phi_0$. Moreover, this value is largely independent of details. In particular, it is completely independent of v_M, μ, L, and W, though it can depend slightly on finer details such as the degree of asymmetry between the top and bottom surfaces, or between the two edges. Remarkably, $I_M \approx \Delta/\Phi_0$ corresponds to the maximal amount of supercurrent[26] carried by a *single* quantum channel that comes from Majorana states, instead of being carried by those coexisting subgap ABS's. The reason is that *finite-energy* $E < 0$ ABS's on the top and bottom surfaces are both occupied, and hence the small energy splitting of ABS's due to their hybridization at the junction edge does not affect the *total* energy E that is a sum over the energies of all occupied states. In contrast, the splitting of *zero-energy* Majorana states changes E by an amount $\delta E_M \approx \sqrt{v_M \Delta/\ell_B}$ over an interval of phase difference $\delta\theta_0 \approx \pi\lambda_B/L$, which gives rise to the above supercurrent,

$$I_M \approx \frac{2\pi}{\Phi_0}\frac{\delta E_M}{\delta\theta_0} = \Delta/\Phi_0. \tag{4}$$

For a proximity gap from Al SC layer $\Delta = 151\ \mu$eV, $I_M \approx 10$ nA. By comparison, for junctions of a few micrometers in width, such as those measured in Ref. 20, there are roughly $k_F L \approx 10^2$–10^3 quantum channels in the entire junction. Consequently, the Majorana contribution to Josephson current, which dominates near an integer flux quanta, is much smaller than the maximum supercurrent for zero flux quanta. These expectations are born out in detail by numerical simulations of Eq. (2) (see Fig. 3).

The situation is similar when a larger integer number N of magnetic-flux quanta pierce the junction. Here, there are N Josephson vortices, each with a bound Majorana state. For $N \ll \frac{L}{\lambda_B}$, the splitting of these states from tunneling between Majoranas is negligible, except in the vicinity of $\theta_0 \approx \pm\pi$ where Majorana states fuse and annihilate at the edges of the junction. A similar peak-dip current structure is observed for higher integer number of flux N with maximal current $I_M \approx \frac{\Delta}{\Phi_0}$ independent of N, and with the peak (dip) width $\delta\theta \approx \frac{\pi\lambda_B}{N\ell_B}$.

Figure 3 shows the current phase relation for various values of flux through the junction. The Majorana mode contribution only starts to become visible for flux within $\approx$5% of a single flux quantum (see right panel of Fig. 3). This contribution appears initially as a shoulder on the background sinus curve, which strengthens and becomes dominant within

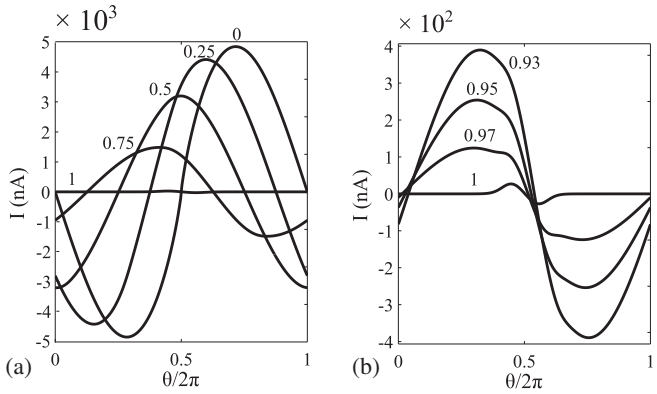

FIG. 3. Current-phase relationship for the parameters listed in Fig. 2 for a wide range of flux (a) Φ and (b) for Φ_B within a few percent of Φ_0. Each curve is labeled by value of Φ_B/Φ_0. The Majorana contribution to the Josephson current becomes appear as a shoulder in the curves of the (b) and eventually dominates close to $\Phi = \Phi_0$.

1% of a single flux quantum. Finally, the critical current I_C as a function of flux through the junction nearly follows the characteristic Frauenhofer pattern, except that I_C does not vanish for integer flux due to the Majorana contributions to the Josephson current (see Fig. 4). In the experiments of Ref. 20, the avoided zero in the Frauenhofer pattern is substantially larger ($\approx$10% of the maximal I_C). As described below, this discrepancy can be explained by accounting for the non-negligible thickness of the TI film in these experiments.

Discussion. Up to now, we have assumed that the thickness h of the TI film is smaller than the size of the Majorana states λ_B. In practice, λ_B is at most a few tens of nanometers. For thicker films with $h > \lambda_B$, the side of the TI may host additional ABS's when the phase difference at the edge is close to π. As shown in Fig. 5, these states will conduct Josephson current, as their energies are sensitive to the phase difference along the sides of the junction. Like the Majorana contribution described above, the contribution of current from these sides can dominate when there are close to an integer number of magnetic-flux quanta piercing the junction. Unlike the Majorana contribution, however, supercurrent from these states exhibits a more conventional sinusoidal current-phase relationship, rather than a sharp peak-dip structure (see Fig. 5).

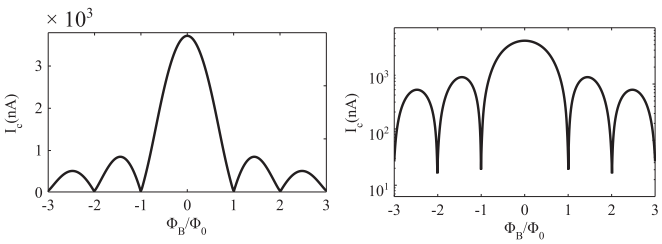

FIG. 4. Critical current I_C as a function of flux, Φ_B in linear (left) and logarithmic (right) scales. The curve is quite close to the conventional Frauenhofer pattern, with the exception that I_C does not vanish at integer numbers of flux quanta due to the extra contribution of the Majorana bound states (as can be seen in the logarithmic scale plot).

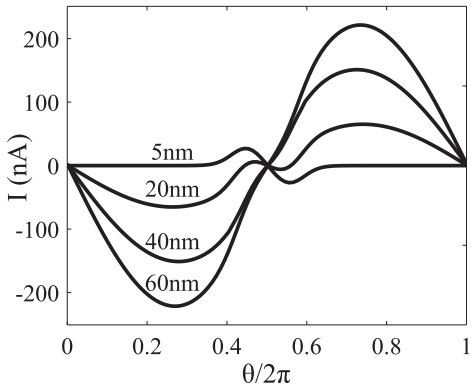

FIG. 5. Current-phase relationship for a single magnetic flux, and varying TI thickness $h = 0$, 20, 40, and 60 nm. Thicker sides tend to contribute conventional Josephson signatures that mask the topological Andreev bound-state contributions.

Therefore, for the purpose of observing Josephson-current signatures of Majorana fermions, it is advantageous to make the TI film as thin as possible without strongly hybridizing the top and bottom surfaces. Since the confinement length in the z direction is only a few nanometers, this last constraint is not too severe. Furthermore, it is advantageous to limit the junction length L (while maintaining $L > \lambda_B$) in order to suppress the conventional Josephson current, which scales as $I \sim L$, in contrast to the width independent contribution from the Majorana bound states.

We have so far neglected any hybridization of the ABS's on the top and bottom surfaces, which may arise from the presence of a noninsulating TI bulk. Such hybridization would create energy splitting of the top and bottom ABS's. However, this splitting is likely very tiny due to Fermi momentum mismatch in the top and bottom surfaces[15] and is not expected to play an important role.

Throughout this work, we have implicitly assumed that the system is in its ground state. Finite temperature will not qualitatively alter our results, provided $T < \delta E_M$. Deviations from ground-state behavior may also occur due to sources of single electrons, such as localized impurity states near the junction. When the Majorana states are far from the junction edge, their mutual fermion parity can be switched by tunneling to local single-electron sources. After such a parity switching, the Majorana modes will follow the positive energy branch as they approach the junction boundary and fuse, thereby contributing the opposite sign of Josephson current compared to the equilibrium case discussed above. Such parity switching events can thereby lead to hysteretic current-phase behavior, whose observation would provide strong evidence for the Majorana character of the Andreev bound states in the junction.

Acknowledgments. We thank Pouyan Ghaemi, Patrick A. Lee, Joel Moore, and especially Bertrand I. Halperin for useful discussions. ACP acknowledges funding from DOE Grant No. DEFG0203ER46076 and also thanks the Kavli Institute for Theoretical Physics at UC Santa Barbara, supported in part by the NSF Grant No. NSF PHY11-25915, for hosting part of this research. LF is partly supported by the US Department of Energy, Office of Basic Energy Sciences, Division of Materials Sciences and Engineering under Award No. 022090-001.

[1]N. Read and D. Green, Phys. Rev. B **61**, 10267 (2000).
[2]D. A. Ivanov, Phys. Rev. Lett. **86**, 268 (2001).
[3]A. Y. Kitaev, Phys. Usp. **44**, 131 (2001).
[4]H. J. Kwon, K. Sengupta, and V. M. Yakovenko, Low Temp. Phys. **30**, 613 (2004).
[5]L. Fu and C. L. Kane, Phys. Rev. B **79**, 161408(R) (2009).
[6]K. T. Law, Patrick A. Lee, and T. K. Ng, Phys. Rev. Lett. **103**, 237001 (2009).
[7]L. Fu, Phys. Rev. Lett. **104**, 056402 (2010).
[8]C. Beenakker, Annu. Rev. Con. Mat. Phys. **4**, 113 (2013).
[9]J. Alicea, Rep. Prog. Phys. **75**, 076501 (2012).
[10]L. Fu and C. L. Kane, Phys. Rev. Lett. **100**, 096407 (2008).
[11]A. C. Potter and P. A. Lee, Phys. Rev. B **83**, 184520 (2011).
[12]P. Zareapour, A. Hayat, S. Yang, F. Zhao, M. Kreshchuk, A. Jain, D. C. Kwok, N. Lee, S. W. Cheong, Z. Xu, A. Yang, G. D. Gu, S. Jia, R. J. Cava, and K. S. Burch, Nat. Commun. **3**, 1056 (2012).
[13]A. Cook and M. Franz, Phys. Rev. B **84**, 201105(R) (2011).
[14]R. Ilan, J. H. Bardarson, H.-S. Sim, and J. E. Moore, arXiv:1305.2210.
[15]See Supplemental Material at http://link.aps.org/supplemental/10.1103/PhysRevB.88.121109 for a discussion, using methods from Ref. 27, of how superconductivity is transmitted from top to bottom surfaces of the TI through the bulk, and explaining why the coupling between Majorana states in the top and bottom surfaces is negligible away from the edge of the junction.
[16]M. Wang *et al.*, Science **336**, 52 (2012).
[17]B. Sacepe, J. B. Oostinga, J. Li, A. Ubaldini, N. J. G. Couto, E. Giannini, and A. F. Morpurgo, Nat. Commun. **2**, 575 (2011).
[18]D. Zhang, J. Wang, A. M. DaSilva, J. S. Lee, H. R. Gutierrez, M. H. W. Chan, J. Jain, and N. Samarth, Phys. Rev. B **84**, 165120 (2011).
[19]M. Veldhorst, M. Snelder, M. Hoek, T. Gang, V. K. Guduru, X. L. Wang, U. Zeitler, W. G. van der Wiel, A. A. Golubov, H. Hilgenkamp, and A. Brinkman, Nat. Mater. **11**, 417 (2012).
[20]J. R. Williams, A. J. Bestwick, P. Gallagher, S. S. Hong, Y. Cui, A. S. Bleich, J. G. Analytis, I. R. Fisher, and D. Goldhaber-Gordon, Phys. Rev. Lett. **109**, 056803 (2012).
[21]F. Qu, F. Yang, J. Shen, Y. Ding, J. Chen, Z. Ji, G. Liu, J. Fan, X. Jing, C. Yang, and L. Lu, Sci. Rep. **2**, 339 (2012).
[22]S. Cho, B. Dellabetta, A. Yang, J. Schneeloch, Z. Xu, T. Valla, G. Gu, M. J. Gilbert, and N. Mason, arXiv:1209.5830.
[23]E. Grosfeld and A. Stern, Proc. Natl. Acad. Sci. USA **108**, 11810 (2011).
[24]Flux expulsion from the superconductors can concentrate flux into the junction region. Consequently, the magnetic flux through the junction, Φ_B, defines an effective area $A_{\rm eff} = \Phi_B/B$, which is in general different than the geometry area $W \times L$.
[25]M. Titov and C. W. J. Beenakker, Phys. Rev. B **74**, 041401(R) (2006).
[26]C. W. J. Beenakker and H. van Houten, Phys. Rev. Lett. **66**, 3056 (1991).
[27]Andrew C. Potter and Patrick A. Lee, Phys. Rev. B **85**, 094516 (2012).